Mathematical Biosciences and Engineering

MBE, 17(5): 4706–4717.
DOI: 10.3934/mbe.2020258
Received: 25 April 2020
Accepted: 23 June 2020
Published: 08 July 2020

http://www.aimspress.com/journal/MBE

Research article

Optimization of fractal dimension and shape analysis as discriminators of erythrocyte abnormalities. A new approach to a reproducible diagnostic tool

Mohamed A Elblbesy [1,2,*] and Mohamed Attia [3,4]

[1] Department of Medical Laboratory Technology, Faculty of Applied Medical Science, University of Tabuk, Saudi Arabia
[2] Department of Medical Biophysics, Medical Research Institute, Alexandria University, Egypt
[3] Department of Biomedical Engineering, Medical Research Institute, Alexandria University, Egypt
[4] Institute for Intelligent Systems Research and Innovation (IISRI), Deakin University, Geelong, Australia

*** Correspondence**: Email: melblbesy@ut.sdu.sa.

Abstract: Manual microscopic analysis is the gold standard for analyzing blood smear. Microscopic analysis of blood smear by a hematologist is subjected to many challenges such as inter-observer variations, operator experience, and conditions of observation. This study aims to examine several parameters extracting from the features of blood smear images. These parameters were used to develop a predictive function, which can be used to automate the microscopic analysis of blood cells instead of manual observation. Fractal dimension, roundness, and aspect ratio were estimated for two types of abnormal erythrocytes: echinocyte and sickle cell. Standard conditions and the choosing of the optimum parameters through the imaging preprocessing were done in order to ensure that the chosen parameters reflect the morphological characteristics of examined erythrocytes. Statistical discriminant analysis was used to build the predictive function for erythrocytes morphological change by a linear combination of the measured parameters. The measured fractal dimensions were 1.825 ± 0.008, 1.502 ± 0.019 and 1.620 ± 0.018 for control, echinocyte, and sickle cell, respectively. The roundness values were 0.94 ± 0.05, 0.83 ± 0.04 and 0.56 ± 0.02 for control, echinocyte, and sickle cell, respectively. The aspect ratio values were 1.005 ± 0.151, 1.046 ± 0.089 and 1.742 ± 0.162 for control, echinocyte, and sickle cell, respectively. The differences between the image analysis parameters for echinocyte and sickle, when compared to control, were statistically significant. The constructed discriminant function using measured parameters was effectively differentiating between examined erythrocytes. The results demonstrated that the selected image analysis parameters extracted from microscopic images with conjunction with statistical discriminant analysis could be used as powerful tools in the classification of erythrocytes according to their morphological characteristics. The findings of this study, in addition to the previous attempts in this filed, could help in the enhancement of a fully automated microscopic

system for blood smear analysis.

Keywords: fractal; roundness; aspect ratio; erythrocyte; echinocyte; sickle cell

1. Introduction

The shape transformation of erythrocytes is of great interest in the field of hematology since several clinical conditions are associated with erythrocytes shape alterations [1,2]. Microscopic observation of blood smear is still the gold standard for blood cell analysis. It is a time-consuming procedure and needs technical expertise to interpret what can be seen in the blood smear [3]. Recently hematological analyzers with automated image analysis systems have been introduced and become a new technology in pathology [4,5]. Once images are digitized, computer applications can be used to analyze the included information. Several tools, such as assisted image analysis and multispectral image analysis, have been developed that promise to improve accuracy, reliability, specificity, productivity—moreover, spatial and spectral image information to classify image contents [6].

Quantitative image analysis is becoming a vital technique for biological experiments. Recently many automated image analysis methods have been developed to quantify the contents of biological images [7]. Many parameters are needed to be extracted from the biological images, such as the number, size, and shape of the cells. A productive collaboration between biologists and imaging processing experts and algorithm developer has been established in order to develop imaging processing tools could be used effectively in the biological-image analysis [8]. Fractal analysis is commonly used in physics, image processing, and medical sciences [9]. Cancer research and medical images analysis are examples for which fractal analysis has proved its utility [10-13]. The fractal-based techniques have been applied in many areas of digital image processing, such as image segmentation, image analysis, image synthesis, computer graphics, and texture coding[14,15]. Based on the fractal theory, image context can be constructed by a set of model parameters that require fewer bits to describe than the original image [16,17]. Fractals are a rough, complex geometric shape that can be subdivided into parts. The fractals can be described using fractal measure (K) and fractal dimension (FD) [16,18–26]. There are different methods to estimated FD, such as walking divider method, box-counting, and fractional Brownian motion [27]. Box-counting is the most straightforward method algorithm for computing FD of 1D and 2D objects [28-30]. It works by covering fractal (its image) with boxes (squares) and then evaluating how many boxes are needed to cover fractal completely. Repeating this measurement with different sizes of boxes will result in the logarithmical function of box size (x-axis) and several boxes needed to cover fractal (y-axis). The Box dimension is taken as an appropriate approximation of the fractal dimension [16,31].

This study aims to evaluate the use of fractal dimension and shape descriptors in the analysis of erythrocytes images and examine their efficiency in the microscopic differentiation of erythrocytes. This is in addition to creating a discriminant model for testing that estimated parameters could be used as predictors for the morphology of erythrocytes.

2. Materials and methods

2.1. Sample collection and preparation

Blood smear slides were collected from different medical laboratories that were already diagnosed, and It had confirmed to contain the desired erythrocytes. The slides were classified according to the erythrocyte's abnormalities into three groups: Group 1: control erythrocytes, Group 2: echinocyte, and Group 3: sickle cells. Images were captured from each blood smear slide with a digital microscopic system consists of a compound light microscope (Leica DM300, Leica-microsystem), eyepiece CCD camera, and computer. The images were captured under a 100X oil-immersed lens and with the magnification of 1000X. The native resolution of the images taken was 128 × 128 pixels (0.064 × 0.064 μm) in TIFF format. Automated imaging analysis of erythrocytes was done in three stages: preprocessing, segmentation, and fractal and shape descriptors analysis. MATLAB (MathWorks. (2011)) was used for image preprocessing, and segmentation while ImageJ was used in fractal analysis and shape descriptors determination [29]. Figure 1 showed the summary of the imaging preprocessing and processing procedures done in this study.

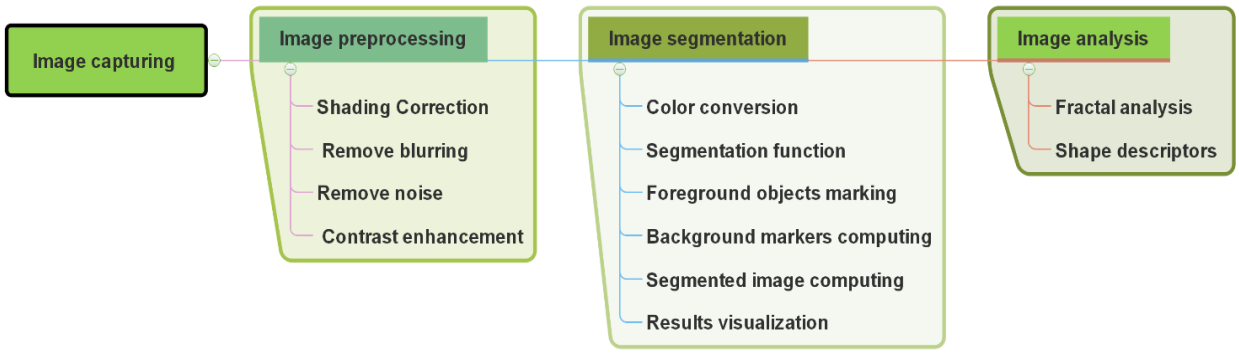

Figure 1. The erythrocytes image processing procedures.

2.2. Imaging preprocessing and segmentation

All images were processed and analyzed were generated in RGB color format, which is challenging to be segmented [32]. Thus, we converted these images into grayscale to facilitate image segmentation. The cell segmentation process was done based on the analysis of the image's histogram to identify the two major classes present in the image, foreground "the cells" (our region of interest (ROI)) and background. The background intensity values tend to be higher intensity, while the foreground was darker than the background, as shown in Figure 2. The optimal threshold for image segmentation was estimated based on the image histogram to minimize the intra-class intensity variance "homogeneity" and increase inter-classes variance between the background and the foreground. All images were converted to 8-bit grayscale. Then auto-correction of the brightness/contrast was done. The contrast enhancement helps in accurately specify an optimal threshold for segmentation. The blood smear images have Bi-modal histogram distribution. One of the peaks represents the cells, and the other represents the background, as shown in Figure 2. By contrast enhancement, the separation between the two peaks was increased.

Otsu's segmentation method is one of the popular segmentation methods that can efficiently segment the foreground from the background based on the image histogram [33]. Using the Otsu method, a robust threshold is estimated based on the enhanced histogram [34]. The optimal threshold is found using an exhaustive search based on all possible threshold values from 0 (minimum intensity value) to 255 (maximum intensity value). It shall minimize the intra-class class variability for both the

background and foreground. For each threshold value "t" the homogeneity is calculated as follows:

$$\sigma_w^2(t) = \omega_0(t)\sigma_0^2(t) + \omega_1(t)\sigma_1^2(t) \quad (1)$$

where $\sigma_w^2(t)$is the homogeneity metric and $\omega_0(t)$are the $\omega_1(t)$ class probability for the foreground and the background. It is calculated from the histogram using L bins as follows:

$$\omega_0(t) = \sum_{i=0}^{t-1} p(i) \quad (2)$$

$$\omega_1(t) = \sum_{i=t}^{L-1} p(i) \quad (3)$$

$\sigma_0^2(t)$ and $\sigma_1^2(t)$ are the in-class variance. To accelerate the estimation process, inter-class variance is calculated as follows:

$$\sigma_b^2(t) = \sigma^2 - \sigma_w^2(t) = \omega_0(\mu_0 - \mu_T)^2 + \omega_1(\mu_1 - \mu_T)^2$$
$$= \omega_0(t)\omega_1(t)[\mu_0(t) - \mu_1(t)]^2 \quad (4)$$

Thus, the objective is to maximize $\sigma_b^2(t)$ instead of minimizing and $\sigma_w^2(t)$

$$\mu_0(t) = \frac{\sum_{i=0}^{t-1} ip(i)}{\omega_0(t)} \quad (5)$$

$$\mu_1(t) = \frac{\sum_{i=t}^{L-1} ip(i)}{\omega_1(t)} \quad (6)$$

$$\mu_T = \sum_{i=0}^{L-1} ip(i) \quad (7)$$

The objective is to find "t" to maximize $\sigma_b^2(t)$ to successfully separate the foreground from the background. Furthermore, a smooth convex hull envelope is estimated to surround each cell to overcome the artifacts in the segmentation due to under segmentation. Then, the small objects in the image were removed using morphological operations on two steps. First, we used the opening operator to remove the small objects. Secondly, the images were dilated to compensate for the opening process. Finally, each cell is individually labeled in the input image. We estimated the size of the surrounding box for each cell, as shown in Figure 3. Based on the estimated bounding boxes, cells were cropped from the input image to be processed individually, as shown in Figure 4.

2.3. Fractal dimension

The fractal dimension (FD) was calculated for the segmented cells using the Box counting method. The cell edge boundary was extracted by edge detection technique. A grid of N squares was superimposed over the edges. The boxes occupied the cell edge were counted. The Hausdorff fractal dimension (FD) was calculated as the following:

$$FD = \frac{\log(N)}{\log(N(s))} \quad (7)$$

where, N is the number of squares in the superimposed grid, and $N(s)$ is boxes.

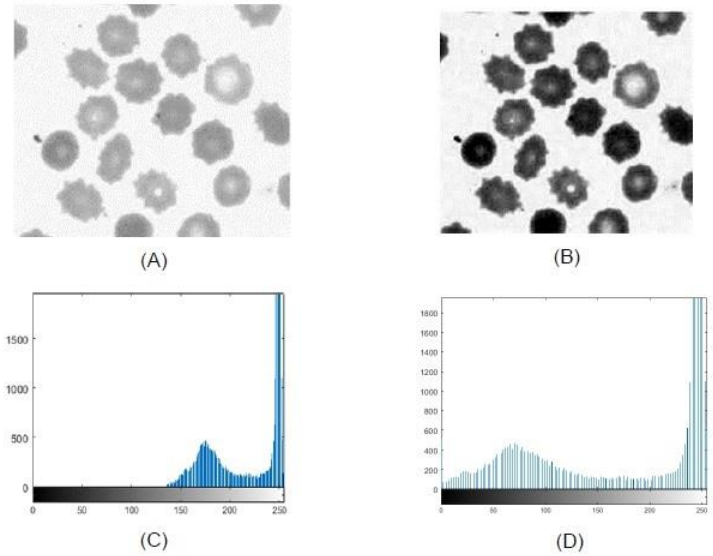

Figure 2. Contrast Enhancement for the grayscale image. The grayscale image in (A) is preprocessed for contrast enhancement in (B). The histogram distribution became bi-modal as the separation between the image object is more obvious.

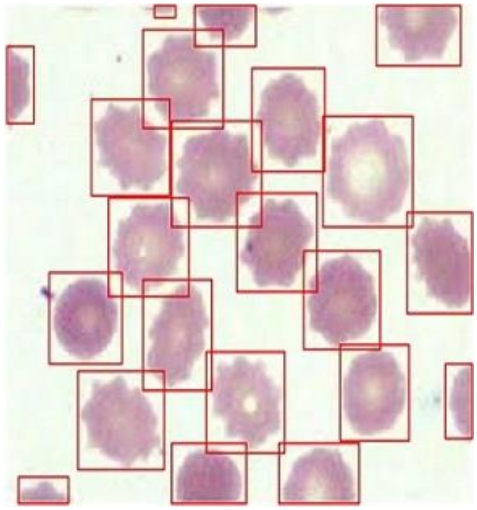

Figure 3. Bounding boxes around each cell.

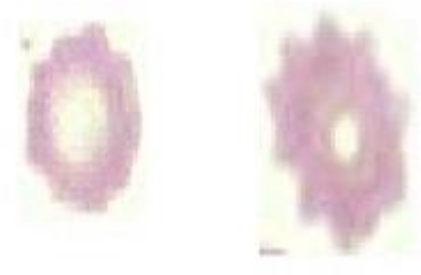

Figure 4. Individual cells are segmented and cropped from the original image.

2.4. Shape descriptors

The segmented cells were represented with none zero pixels from the binary equivalent image. The shape features measured in this study were region and boundary-based. The features determined were roundness (RO) and aspect ratio (AR). RO and AR were estimated by the following formulas:

$$RO = 4 \times \frac{cell\ area}{\pi \times Cell\ Major\ axis} \quad (8)$$

$$AR = \frac{Cell\ major\ axis}{Cell\ minor\ axis} \quad (9)$$

2.5. Statistical analysis

All the parameters were presented as mean ± SD. The statistical significance was considered as $p < 0.001$. FD, RO, and AR were used as a predictor variable to build a discriminant model [35]. The proposed discriminant analysis formed from the composition of canonical discriminant functions of a linear combination of independent predictor variables. Predicator equations (PE) were built by the coefficients of predictor variables, which were the Fisher linear functions [35]. Casewise testing was performed to check the validity of PE. IBM SPSS 23 was used to perform statistical analysis.

3. Results and discussion

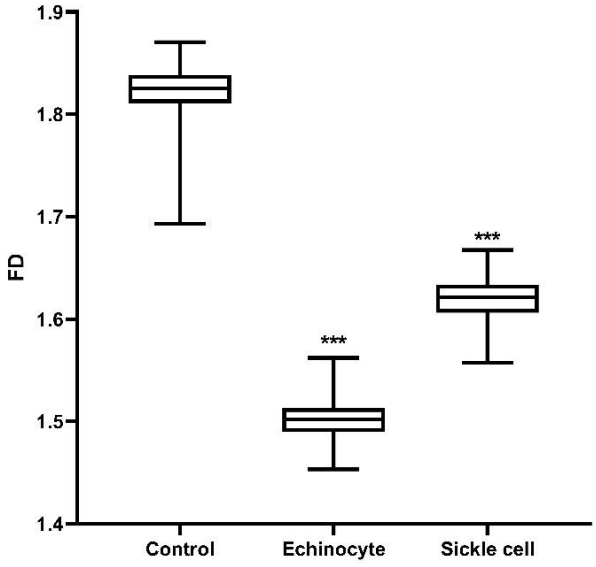

Figure 5. Fractal dimension of echinocyte and sickle cell compared to control. *** statistically highly significant as $P < 0.001$.

Human erythrocytes were used in this study to examine that fractal dimension and shape descriptors parameters could reflect well the morphological characteristics of normal and abnormal erythrocytes. One hundred erythrocytes for each group were used in this study to be analyzed by the suggested image analysis parameters. As shown in Figure 5, FD for control was 1.825 ± 0.008, while it was 1.502 ± 0.019 and 1.620 ± 0.018 for echinocyte, and sickle cell, respectively. RO was 0.94 ±

0.05, 0.83 ± 0.04 and 0.56 ± 0.02 for control, echinocyte, and sickle cell, respectively. As shown in Figure 6, the difference between RO of control and echinocyte and the sickle cell was highly significant. The aspect ratio values were 1.005 ± 0.151, 1.046 ± 0.089 and 1.742 ± 0.162 for control, echinocyte, and sickle cell, respectively, and the differences were statistically significant, as shown in Figure 7.

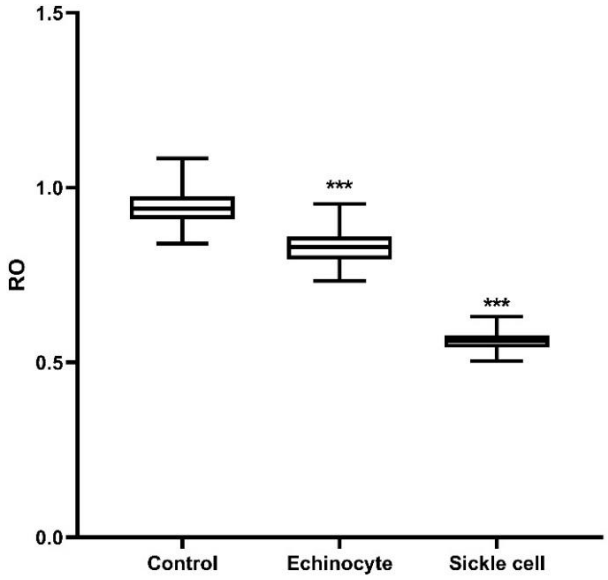

Figure 6. Roundness of echinocyte and sickle cell compared to control. *** statistically highly significant as $P < 0.001$.

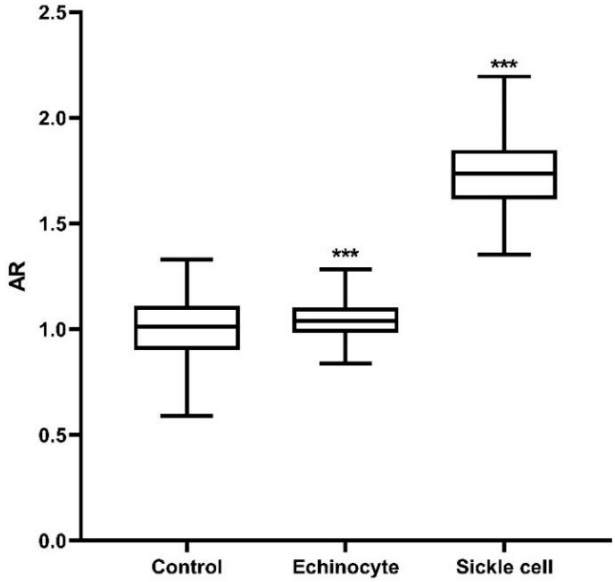

Figure 7. Aspect ratio of echinocyte and sickle cell compared to control. *** statistically highly significant as $P < 0.001$.

The normality test of FD, RO, and AR showed that they were normally distributed. As normality is the prerequisite of discriminant analysis, FD, RO, and AR for the three examined groups were suitable to be used as discriminators parameters. Table 1 shows the two canonical discriminant functions. The discriminant analysis showed that the two discriminant functions cumulatively accounted for 100 % of the variance. Thus, these two functions could represent the suggested predictive model correctly. Table 2 represents the links between the canonical functions and the original variable by introducing the structure matrix of the model. A strong positive correlation was indicated between FD and first function, while the strong negative correlation between RO and second function was reported. A moderate correlation between AR and second function was reported. Fisher's function coefficients are listed in Table 3. These coefficients were used to build the predictor equation (PE) as the following [36]:

$$PE = FD.Coef_{FD} + RO.Coef_{RO} + AR.Coef_{AR} + constant \qquad (10)$$

where $Coef_{FD}$ is the group classification coefficient of FD , $Coef_{RO}$ is the group classification coefficient of RO, and $Coef_{AR}$ is the group classification coefficient of AR.

PE was used in erythrocytes classification. The classification of the erythrocyte, according to the suggested model, was originated from the substitution for FD, RO, and AR and their coefficients given in Table 3 in equation 10. Classification of the erythrocytes was done according to the largest PE value. The summary of the classification results of casewise testing is reported in Table 4. The comparison between the observed and predicted erythrocytes was 96%, 94%, and 98 % for control, echinocyte, and sickle cell, respectively. The coefficient of the agreement was 0.75 (95% confidence interval, $p < 0.001$). In this study, evaluation of using imaging processing software in conjunction with the statistical tool was presented. Our results showed that the predictor function originated from the discriminant analysis effectively classified erythrocytes according to their morphological characteristics. Thus the discriminant analysis is proven to be a powerful statistical tool that overcomes the deficiency in the corresponding analysis tools [37,38]. The imaging analysis in this study was performed using two different applications MATLAB and ImageJ. This may be considered as a drawback of this study. Image segmentation is the most critical step in imaging processing, as well as choosing the ROI. We applied image segmentation by MATLAB to get reliable results with high efficiency due to the options offered in MATLAB. ImageJ was used in this study to estimate the fractal dimension and shape descriptors of erythrocytes. ImageJ offered considerable sensitivity and specificity in the morphological analysis of erythrocytes. The automated cell morphometric method based on discriminant analysis was suggested by Albertini et al. [36]. Their model was based on the morphometric parameters such as chromogenic index and density profile extracted from the image processing of erythrocytes [36]. The same analytical method was used in this study but with different predictor variables. By using FD with other shape descriptors from three different erythrocyte cell shape morphologies, three PE were constructed. PE sensitivity and specificity were higher than other classification functions used in the previous studies [36]. This can be explained as we entered the fractal dimension in the analysis with other shape descriptors. FD was used before to study living cells and tissues in different pathogenic cases [39-41]. Fractal analysis expresses well the details of the exterior features of the object [40,42]. The fractal dimension was one of the predictor variables used in the present study and improved remarkably the suggested classification PE results.

Table 1. Summary of the predictor functions.

Function	Eigenvalue	% of Variance	Cumulative %	Canonical Correlation
1	53.173[a]	78.3	78.3	0.991
2	14.705[a]	21.7	100.0	0.968

a. First 2 canonical discriminant functions were used in the analysis.

Table 2. Structure matrix of predictor model.

Variables	Function1	Function2
FD	0.857*	0.507
RO	0.365	-0.744*
AR	-0.163	0.561*

Pooled within-groups correlations between discriminating variables and standardized canonical discriminant functions
Variables ordered by absolute size of correlation within function.
**. Largest absolute correlation between each variable and any discriminant function.*

Table 3. Classification function coefficients.

Variables	Type		
	Control	Echinocyte	Sickle cell
FD	4524.468	3725.123	3957.578
RO	806.539	694.857	555.051
AR	12.752	22.147	55.269
(Constant)	-4517.802	-3098.574	-3410.204

Fisher's linear discriminant functions.

Table 4. Classification summary using the predictor function.

		Predicted Group Membership			
	Type	Control	Echinocyte	Sickle cell	Total
Count %	Control	96 %	4 %	0	100 %
	Echinocyte	4 %	94 %	2 %	100 %
	Sickle cell	0 %	2 %	98 %	100 %

4. Conclusion

The fractal analysis and shape descriptors in the present study reflected well the morphological characteristics of the erythrocytes. The discriminant analysis using fractal dimension and morphological parameters improved classifications results of erythrocytes. The method suggested in this study provides a suitable tool with high sensitivity and specificity to differentiate erythrocytes.

Acknowledgment

The authors would like to acknowledge the financial support of this work from the Deanship of Scientific Research (DSR), University of Tabuk (Tabuk, Saudi Arabia, under grant no. (S-1439-0133)).

This study was done under the approval of the Research Ethics Committee, University of Tabuk (Approval No. UT-71-19-2018).

Conflict of interest

Authors declare no conflict of interest in this paper.

References

1. B. Constantino, Reporting and grading of abnormal red blood cell morphology, *Int. J. Lab. Hematol.*, **37** (2015), 1–7.
2. J. Ford, Red blood cell morphology, *Int. J. Lab. Hematol.*, **35** (2013), 351–357.
3. M. Buttarello, M. Plebani, Automated blood cell counts: state of the art, *Am. J. Clin. Pathol.*, **130** (2008), 104–116.
4. L. Da Costa, Digital image analysis of blood cells, *Clin. Lab. Med.*, **35** (2015), 105–122.
5. L. Pantanowitz, Digital images and the future of digital pathology, *J. Pathol. Inform.*, **1** (2010), 15.
6. I. Mansoor, C. Zalles, F. Zahid, K. Gossage, R. M. Levenson, D. L. Rimm, Fine-needle aspiration of follicular adenoma versus parathyroid adenoma, *Cancer Cytopathol.*, **114** (2008), 22–26.
7. H. Peng, Z. Ruan, F. Long, J. H. Simpson, E. W. Myers, V3D enables real-time 3D visualization and quantitative analysis of large-scale biological image data sets, *Nat. Biotechnol.*, **28** (2010), 348–353.
8. A. H. K. Roeder, A. Cunha, M. C. Burl, E. M. Meyerowitz, A computational image analysis glossary for biologists, *Development*, **139** (2012), 3071–3080.
9. N. A. Davies, N. K. Harrison, R. H. Morris, S. Noble, M. J. Lawrence, L. A. D'Silva, et al., Fractal dimension (df) as a new structural biomarker of clot microstructure in different stages of lung cancer, *Thromb. Haemost.*, **114** (2015), 1251–1259.
10. A. R. Backes, L. C. Gerhardinger, E. Batista Neto Jdo, O. M. Bruno, Medical image retrieval and analysis by Markov random fields and multi-scale fractal dimension, *Phys. Med. Biol.*, **60** (2015), 1125–1139.
11. Z. Ali, I. Elamvazuthi, M. Alsulaiman, G. Muhammad, Detection of voice pathology using fractal dimension in a multiresolution Analysis of Normal and Disordered Speech Signals, *J. Med. Syst.*, **40** (2016), 20.
12. G. Mohan and M. M. Subashini, MRI based medical image analysis: Survey on brain tumor grade classification, *Biomed. Signal Process*, **39** (2018), 139–161.
13. A. Bitler, R. S. Dover, Y. Shai, Fractal properties of cell surface structures: A view from AFM; 2018. Elsevier. pp. 64–70.
14. G. Landini, Fractals in microscopy, *J. Microsc.*, **241** (2011), 1–8.
15. B. Yao, F. Imani, A. S. Sakpal, E. Reutzel, H. Yang, Multifractal analysis of image profiles for the characterization and detection of defects in additive manufacturing, *J. Manuf. Sci. Eng.*, **140** (2018), 031014.
16. T. F. Nonnenmacher, G. Baumann, A. Barth, G. A. Losa, Digital image analysis of self-similar cell profiles, *Int. J. Biomed. Comput.*, **37** (1994), 131–138.

17. K. Harrar, R. Jennane, K. Zaouchi, T. Janvier, H. Toumi, E. Lespessailles, Oriented fractal analysis for improved bone microarchitecture characterization, *Biomed. Signal Process*, **39** (2018), 474–485.
18. B. a. K. T. Venkatalakshmi, Automatic red blood cell counting using Hough transform, *2013 IEEE Conference on Information & Communication Technologies (ICT)* (2013).
19. M. Habibzadeh, A. Krzyżak, T. Fevens, Comparative study of shape, intensity and texture features and support vector machine for white blood cell classification, *J. Theor. Appl. Comput. Sci.*, **7** (2013), 20–35.
20. E. A. Mohammed, M. M. Mohamed, B. H. Far, C. Naugler, Peripheral blood smear image analysis: A comprehensive review, *J. Pathol. Inform.*, **5** (2014), 9.
21. G. De Vico, V. Peretti, G. A. Losa, Fractal organization of feline oocyte cytoplasm, *Eur. J. Histochem.*, **49** (2005), 151–156.
22. B. B. Mandelbrot *The fractal geometry of nature*. New York: W.H. Freeman. 1983, pp. 468.
23. E. R. Weibel, Fractal geometry: A design principle for living organisms, *Am. J. Physiol.*, **261** (1991), L361–369.
24. J. W. Fuseler, J. P. Robichaux, H. I. Atiyah, A. F. Ramsdell, Morphometric and fractal dimension analysis identifies early neoplastic changes in mammary epithelium of MMTV-cNeu mice, *Anticancer Res.*, **34** (2014), 1171–1177.
25. W. Sumelka, Fractional calculus for continuum mechanics–anisotropic non-locality, *Bull. Pol. Ac. Tech.*, **64** (2016), 361–372.
26. X. Zhang, Y. Xu, R. L. Jackson, An analysis of generated fractal and measured rough surfaces in regards to their multi-scale structure and fractal dimension, *Tribol. Int.*, **105** (2017), 94–101.
27. A. Annadhason, Methods of fractal dimension computation, *IRACST*, **2** (2012).166–169.
28. R. D. Peng, H. P. Xie, Y. Ju, Computation method of fractal dimension for 2-D digital image, *J. China Univ. Min. Technol.*, **33** (2004), 19–24.
29. C. T. Rueden, J. Schindelin, M. C. Hiner, B. E. DeZonia, A. E. Walter, E. T. Arena, et al., ImageJ2: ImageJ for the next generation of scientific image data, *BMC Bioinform.*, **18** (2017), 529.
30. S. R. Nayak, J. Mishra, P. mohan Jena, Fractal analysis of image sets using differential box counting techniques, *Int. J. Inform. Technol.*, **10** (2018), 39–47.
31. L. S. Liebovitch, T. Toth, A fast algorithm to determine fractal dimensions by box counting, *Phys. Letters*, **141** (1989), 386–390.
32. T. Markiewicz, M. Dziekiewicz, S. Osowski, M. Maruszynski, W. Kozlowski, R. Boguslawska-Walecka, Thresholding techniques for segmentation of atherosclerotic plaque and lumen areas in vascular arteries, *Bull. Pol. Ac. Tech.*, **63** (2015), 269–280.
33. T. Y. Goh, S. N. Basah, H. Yazid, M. J. A. Safar, F. S. A. Saad, Performance analysis of image thresholding: Otsu technique, *Measurement*, **114** (2018), 298–307.
34. N. Otsu, A threshold selection method from gray-level histograms, *IEEE Transact. Syst. Man Cybernet.*, **9** (1979), 62–66.
35. M. J. Anderson, A new method for non-parametric multivariate analysis of variance, *Austral Ecol.*, **26** (2001), 32–46.
36. M. C. Albertini, L. Teodori, E. Piatti, M. P. Piacentini, A. Accorsi, M. B. Rocchi, Automated analysis of morphometric parameters for accurate definition of erythrocyte cell shape, *Cytometry A.*, **52** (2003), 12–18.

37. Z. Liang, P. Shi, An efficient and effective method to solve kernel Fisher discriminant analysis, *Neurocomputing*, **61** (2004), 485–493.
38. R. Singh, N. Rajpal, R. Mehta, Dynamic ECG Classification Using Shift-Invariant DTCWT and Discriminant Analysis. *Proceedings of ICETIT 2019*: Springer. (2020), pp. 490–500.
39. V. V. Revin, A. A. Ushakova, N. V. Gromova, L. A. Balykova, E. S. Revina, V. V. Stolyarova, et al., Study of Erythrocyte Indices, Erythrocyte Morphometric Indicators, and Oxygen-Binding Properties of Hemoglobin Hematoporphyrin Patients with Cardiovascular Diseases, *Adv. Hematol.*, **2017** (2017).
40. M. Stankovic, I. Pantic, D. E. L. SR, N. Puskas, I. Zaletel, S. Milutinovic-Smiljanic, et al., Quantification of structural changes in acute inflammation by fractal dimension, angular second moment and correlation, *J. Microsc.*, **261** (2016), 277–284.
41. F. M. Smits, C. Porcaro, C. Cottone, A. Cancelli, P. M. Rossini, F. Tecchio, Electroencephalographic fractal dimension in healthy ageing and Alzheimer's disease, *PLoS One*, **11** (2016), e0149587.
42. J. Pribic, J. Vasiljevic, K. Kanjer, Z. N. Konstantinovic, N. T. Milosevic, D. N. Vukosavljevic, et al., Fractal dimension and lacunarity of tumor microscopic images as prognostic indicators of clinical outcome in early breast cancer, *Biomark. Med.*, **9** (2015), 1279–1277.